

Better Alloys with Quantum Design

Travis E. Jones,^{1,2} Mark E. Eberhart,^{1,*} Scott Imlay,^{1,3} Craig Mackey,^{1,3} and Greg B. Olson⁴

¹*Molecular Theory Group, Colorado School of Mines, Golden, Colorado 80401, USA*

²*School of Physics, The University of Sydney, Sydney, New South Wales 2006, Australia*

³*Tecplot, Inc., Bellevue, Washington 98015, USA*

⁴*Department of Materials Science and Engineering, Northwestern University, Evanston, Illinois 60208, USA*

(Received 12 July 2012; published 20 September 2012)

Alloy discovery and development is slowed by trial and error methods used to identify beneficial alloying elements. This fact has led to suggestions that integrating quantum theory and modeling with traditional experimental approaches might accelerate the pace of alloy discovery. We report here on one such effort, using advances in first principles computation along with an evolving theory that allows for the partitioning of charge density into chemically meaningful structures, alloying elements that improve the adhesive properties of interfaces common to high strength steels have been identified.

DOI: [10.1103/PhysRevLett.109.125506](https://doi.org/10.1103/PhysRevLett.109.125506)

PACS numbers: 81.05.Bx, 62.20.mm

The search for alloying elements to improve mechanical properties is largely empirical, though it is known that effects of these elements result from changes to the alloy charge density. To understand the nature of these changes and accelerate the pace of alloy discovery, investigators are augmenting traditional experimental methods with quantum mechanical calculations. Here we review our efforts to use advanced quantum mechanical methods in combination with an extended form of a topological representation of molecular structure known as the quantum theory of atoms in molecules [1–4] to understand and predictably alter one of the atomic scale interactions that influences the adhesive properties of metal ceramic interfaces common in high strength steels—the ideal work of separation, W_∞ , defined as the thermodynamic minimum energy needed to separate an interface into two free surfaces.

This is a particularly appropriate property for quantum mechanical investigation, for, though difficult to measure, it can be calculated with density functional theory based methods [5]. For example, Wu, Freeman, and Olson [6] used the full-potential linearized augmented plane wave (FLAPW) method to calculate W_∞ and account for the observed strengths of steel boundaries containing B or P; Schweinfest, Paxton, and Finnis [7] have shown that the weakening of Cu boundaries by Bi coincides with a decrease in the work of separation; Geng, Freeman, and Olson [8] calculated W_∞ for a series alloying elements and used the tabulated values as a means of improving alloy chemistry. Though these and many other studies have demonstrated that the calculated ideal work of separation can be used to identify or confirm elements that affect strength, none has provided a means to *predict* these effects. The reason, we believe, is that these studies did not involve a systematic correlation of charge density with changes to W_∞ .

The quantum theory of atoms in molecules provides a powerful formalism through which to systematically in-

vestigate charge density [1]. The theory begins by characterizing the topology of the charge density $\rho(\vec{r})$ by its rank 3 critical points (CPs) the places where $\rho(\vec{r})$ achieves extreme values. As a 3D scalar field, $\rho(\vec{r})$ possesses at most four kinds of CP: local minima, local maxima, and two types of saddle points. These CPs are denoted by an index giving the number of positive curvatures minus the number of negative curvatures. For example, at a minimum CP the curvature in all three orthogonal directions is positive; therefore, it is called a (3, +3) CP. The first number is simply the number of dimensions of the space, and the second is the net number of positive curvatures. A maximum is denoted by (3, -3), because all three curvatures are negative. A saddle point with two of the three curvatures negative is denoted (3, -1), while the other saddle point is a (3, +1) CP.

Bader's extensive studies showed that it was possible to correlate topological properties of $\rho(\vec{r})$ with elements of molecular structure [1,9]. In particular, a bond path was argued to be the ridge of maximum charge density connecting two nuclei. The existence of such a ridge is guaranteed by the presence of a (3, -1) CP and, hence, is referred to as a bond CP. Other types of CPs have been correlated with other features of molecular structure. A (3, +1) CP is required at the center of ring structures and is designated a ring CP. Cage structures must enclose a single (3, +3) CP and are named cage CPs. The locations of the atomic nuclei always coincide with a (3, -3) CP, which is called a nuclear CP.

Bader [1] also showed that a molecule or solid can be partitioned into space filling regions, Bader atoms, in which each region contains a single nucleon bounded by a surface of zero flux in the gradient of the charge density, zero flux surface. By virtue of being bounded by a zero flux surface, the properties of Bader atoms are well defined and additive. That is, molecular properties, e.g., energy, can be expressed as the sum of Bader atom energies.

Later, Eberhart [2] and Jones and Eberhart [3,4] noted that the topology of $\rho(\vec{r})$ can be more fully characterized through the inclusion of charge density ridges. In two dimensions, a ridge is a familiar topographic feature, the gradient path connecting mountain passes to neighboring peaks, for example. This ridge is an extremum with respect to all neighboring paths. Similarly, a valley is the gradient path connecting a saddle point to a local minimum. Because valleys and ridges differ only by the sign of the curvatures along the path, both are referred to as “ridges.” In three-dimensional fields, such as the electron charge density, ridges are both the gradient paths and surfaces that are extreme with respect to all neighboring gradient paths and surfaces. They are denoted by an index, $n-d$, where n is the dimensionality of the space and d is the number of principal directions in which the charge density is extreme [10].

Explicitly including ridges in the description of the topology of $\rho(\vec{r})$ recovers bond paths and Bader atoms while simultaneously providing a richer representation of molecular structure. For example, the bond path is a 1-ridge, and the surface of a Bader atom is composed of 2-ridges. However, there are additional space filling structures bounded by 2-ridges. In particular, there is one such structure that encompasses a single bond point and bond path. We call these regions bond bundles [2–4], and, like Bader atoms, they are bounded by zero flux surfaces and hence possess well defined and additive properties. Among the more obvious and easily computed bond-bundle properties is the number of electrons the bundle contains, and it is this property that we have found correlates with W_∞ .

The system explored in this work is representative of steels strengthened by a ceramic dispersion, typically TiC. During plastic deformation, dislocations are unable to shear the hard ceramic and pile up at the Fe/ceramic interface. These pileups increase the stress at the interface, eventually pulling it apart to produce voids, which then grow. The material fails as these voids link up. Toughness can be enhanced by reducing the number of interfaces that ultimately separate [11], which, in turn, can be achieved by increasing the ideal work of separation of the Fe/ceramic interface.

By choosing this system, we were able to leverage the research of Arthur Freeman and his group at Northwestern University, which was using the highly accurate and resource intensive FLAPW method to perform virtual “tensile tests” on a series of Fe/ceramic interfaces. Of the many interfacial geometries explored, we were concerned with the data from the coherent Fe(001)/(TM1, TM2)C interface with $\langle 100 \rangle_{\text{bcc}} \parallel \langle 110 \rangle_{\text{carbide}}$ orientation, where TM1 and TM2 are each one of the transition metals: V, Mo, Nb, or Ti. In all cases the lattice mismatch between the Fe and the carbide was accounted for by optimizing the iron and ceramic cell volumes, and, as in previous studies on Fe-carbide interfaces, there was a strong carbon site

preference for the Fe atoms [12–14], producing the general equilibrium structure shown in Fig. 1.

The virtual tensile test began by determining the inter-layer spacings of minimum energy. The interfaces were then separated by rigidly displacing the two half crystals (carbide and iron) and then allowing the layers to relax while holding the cell volume fixed. The process was repeated until there was insignificant energy change accompanying further separation. The energy difference between the initial and the fully separated configurations gives W_∞ , which for the Fe/TiC interface was 3.6 J/m^2 .

Recalling that interfacial failure results from dislocation pileups that cause stress to concentrate at the interfaces, any increase in W_∞ will improve toughness by increasing the size of the pileups needed to initiate interfacial debonding. However, the best interface possible is one with an ideal work of separation equal to 4.7 J/m^2 —the work to separate (100) planes of bcc Fe [15]. Increasing interfacial W_∞ beyond this point will not improve properties, as voids will initiate in the Fe lattice. Accordingly, we define ΔW_∞ to be the difference between the ideal work of separation of (100) planes of pure bcc Fe and W_∞ for the ceramic. For the base case of the Fe/TiC interface, $\Delta W_\infty = 1.1 \text{ J/m}^2$. Of the ten carbide interface tested, Fe/VC was found to have the greatest work of separation of 3.78 J/m^2 and a ΔW_∞ of 0.92 J/m^2 , an improvement of 16% over the TiC interface.

Because the charge density is a more robust property than total energy, we used the less computationally demanding Vienna *ab initio* simulation package (VASP) version 4.6 with the Perdew-Burke-Ernzerhof generalized gradient corrections [16,17] to generate $\rho(\vec{r})$ from the FLAPW converged geometries. (Comparisons of the VASP and FLAPW charge densities showed no significant

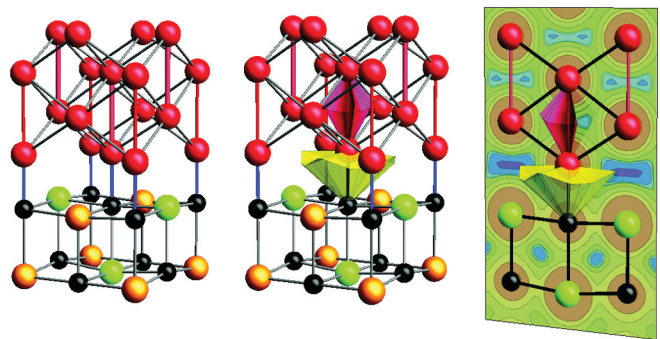


FIG. 1 (color). The Fe(001)/(TM1, TM2)C interface; black spheres represent C, green TM1, orange TM2, and red Fe atoms, and lines are the ridges of maximum charge density, i.e., bond paths. (left) The location of atoms and bond paths. (center) One of the Fe-Fe second-neighbor bond bundles is shaded red and below that the Fe-C interface bond bundle is shaded yellow. (right) A (200) cut plane through the interface depicting the charge density contours and the bond paths, atoms, and selected bond bundles intersecting this plane.

quantitative difference.) The calculated densities were then interrogated with TECPLOT for the locations of bond paths, 2-ridges, and bond bundles.

The topology of the calculated charge density of the unstrained interfaces revealed C-TM1, C-TM2, C-Fe, and Fe-Fe bond paths between all nearest-neighbor atom pairs, independent of the choice of TM1 and TM2. (These bond paths are shown in Fig. 1.) Such first-neighbor bonding topologies are typical of many systems, including bcc Fe [18,19]. However, unlike bulk bcc Fe, second-neighbor Fe-Fe bond paths and bond bundles were also found (Fig. 1).

After determining the zero strain bonding, we investigated its evolution as a function of strain. It is easiest to visualize the effects of interfacial strain on the bond bundles by observing their cross section in a cut plane perpendicular to the interface, as shown in Fig. 2 for an Fe/VVC interface. (This interface is representative of all the interfaces modeled.) The energy versus strain curve is shown at the top of the figure. Consider three regions of this sigmoidal curve: In the first (separations are less than 1.5 Bohr) the curvature is positive, in the second (between 1.5 and 3.5 Bohr) the curvature is approximately zero, and in the final region (separations greater than 3.5 Bohr) the curvature is negative. If we consider only the harmonic contributions to the separation energy, the effective stiffness of

the interface can be inferred from the curvature of the energy versus separation curve, which, not surprisingly, indicates that the interface is softening well into region 3, a phenomenon generally correlated with charge flow [20]. In this case, it appears that the softening is correlated with the flow of charge from and to the Fe-Fe second-neighbor bond bundle, as is evident by examining the lower panel of Fig. 2. Region 1 is characterized by the flow of charge from Fe-Fe second-neighbor to Fe-Fe first-neighbor bond bundles. At the onset of region 2 the second-neighbor bond bundle vanishes. The onset of region 3 coincides with the reformation of the Fe-Fe second-neighbor bond bundle as charge flows from first- to second-neighbor bond bundles. Note that there is no similar correlation with the other bond bundles of the system.

The correlation between charge flow and elastic response is easily rationalized. Focusing on the Fe-Fe second-neighbor bond bundle, by the electrostatic theorem, at equilibrium the repulsion between the Fe nuclei at either end of the second-neighbor bond path is just canceled by their attraction for the intervening electron density. As these nuclei are displaced, the charge flow from the bond bundle descreens the nuclei, softening the bond bundle. In turn, strain is localized in this softening bond bundle, as is clearly visible in Fig. 2 where, until the interfacial separation exceeds 3.5 Bohr, a greater portion of the uniaxial strain is localized in the Fe-Fe second-neighbor bond path than in the C-Fe bond path. Beyond 3.5 Bohr, the second-neighbor bond bundle reforms, screening the repulsion of the Fe nuclei, which causes them to shorten their distance. The energy realized as the second-neighbor bond bundle reforms, and the Fe nuclei move together, does work by lengthening the Fe-C bond bundle, as is evident in Fig. 2

Obviously, the Fe-Fe second-neighbor bond bundle is important to the dynamic response of these interfaces. However, the ideal work of separation depends only on the initial and final states. Hence, we hypothesized that the difference between the number of electrons contained in this bond bundle pre- and postseparation should correlate with the ideal work of separation. As all the second-neighbor bond bundles of the separated systems are identical, W_∞ should depend only on the number of electrons in the interfacial bond bundle. Accordingly, Fig. 3 shows the integrated valence charge densities in the second-neighbor Fe-Fe bond bundles in the mixed Fe-carbide interfaces plotted against the calculated work of fracture. Over this range of data, these two quantities are linearly related. (Emphasizing the significance of the bond bundle, we also sought a correlation between the work of fracture and the value of the charge density at the Fe-Fe second-neighbor bond point, and at the Fe-C bond point; see Supplemental Material [21]. No correlation was found.)

All of these observations point to a structure-property relationship in which the number of electrons in second-

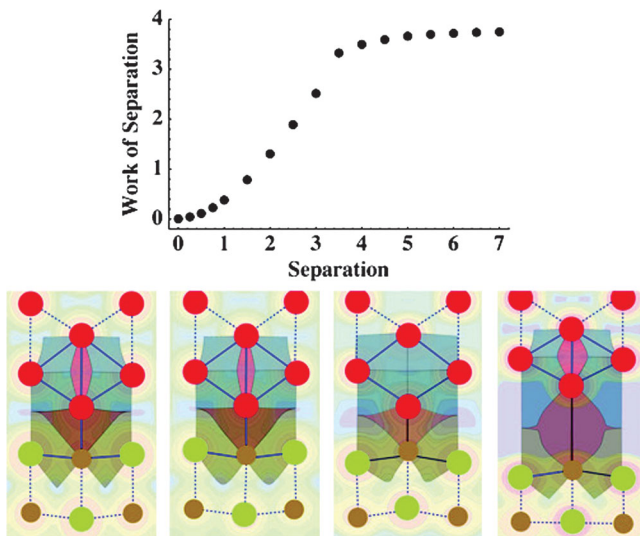


FIG. 2 (color). The work of separation in J/m^2 as a function of separation distance in Bohr. The bottom plots show cross sections of the bond bundles in the (200) plane containing the Fe-Fe second-neighbor and Fe-C first-neighbor bond paths at 0.0 (far left), 0.5 (middle left), 1.5 (middle right), and 3.5 (far right) Bohr separation. As in Fig. 1, the region shaded red gives the cross section in this plane of the Fe-Fe second-neighbor bond bundle, while the region shaded brown gives the cross section in this plane of the Fe-C bond bundle across the interface. Other shading correspond to the cross sections of other bond bundles, which change little through the separation.

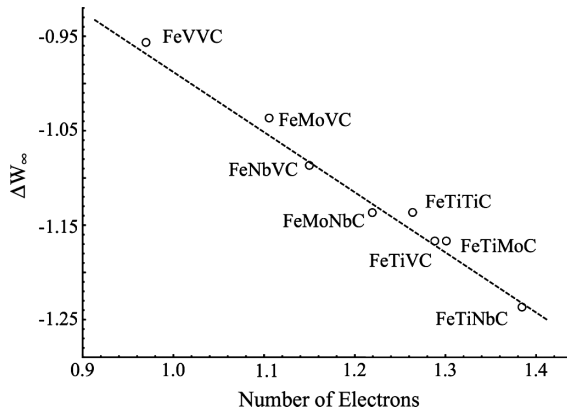


FIG. 3. The difference in the work of separation in J/m^2 as a function of the number of valence electrons in the second-neighbor Fe-Fe bond bundle in the mixed-carbide interfaces, $\text{Fe}(001)/M_1M_2\text{C}$. M_1 and M_2 are each one of the following transition metals: Ti, V, Nb, and Mo.

neighbor Fe-Fe bond bundles controls the ideal work of separation. This structure-property relationship can be used to design the chemistry of an improved interface.

By group theory, only Fe s , p_z , and d_{z^2} atomic orbitals contribute to the second-neighbor Fe-Fe bond path. Our calculations confirm that there is little contribution to the second-neighbor bond bundle from p_z character. In fact, cluster calculations performed with the Amsterdam density functional package [22] show the different occupancies of the second-neighbor bond bundles depicted in Fig. 3 are the result of transition metal induced changes to s - d_{z^2} hybridization. Hence, introduction of p_z orbitals on the Fe site must add out of phase to one lobe of a d_{z^2} and, on that side, will decrease the size of this second-neighbor bond bundle. Nickel is a common substitutional for Fe and known to possess low-lying p character. Hence, we predicted that Ni substituted on Fe sites will reduce the number of electrons in second-neighbor bond bundles and increase W_∞ .

In choosing a substitutional site, we avoided the Fe atom bound to the carbon, as that may lead to changes in site preference and different properties of the bond bundles across the interface. Instead, we substituted the Fe atoms in the third (001) plane in the $\langle 001 \rangle$ direction, the top layer of Fe atoms in Fig. 1.

The work of separation of two different Ni alloyed Fe/VVC interfaces was then calculated with FLAPW to confirm the prediction that a Ni-Fe alloy will yield an interface with a greater ideal work of separation. In the first alloy, Ni atoms were substituted for 100% of the Fe atoms in the third (001) plane in the $\langle 001 \rangle$ direction. In the second, only 50% of these Fe atoms were replaced with Ni. As expected, W_∞ for both alloys was larger than the 3.78 J/m^2 seen in Fe/VVC. The work of adhesion of the 100% alloy increased to 3.79 J/m^2 , while the 50% alloy

displayed a larger increase to 3.86 J/m^2 . We speculate that the difference between the 100% and 50% concentrations derives from Ni-Ni interactions, which will tend to align the p_z orbital parallel to the interface instead of toward second-neighbor bond bundles. As the distance between Ni atoms increases, this trend will decrease. It is likely that a more dilute Ni substitution will further improve W_∞ . Nonetheless, for the 50% case ΔW_∞ is 0.84 J/m^2 —a 24% improvement over the base case. Subsequent FLAPW calculations confirm the Ni atom site preference to be the site investigated.

This newly discovered relationship between bond-bundle occupancy and W_∞ helps to explain the properties of a new high strength low carbon steel known as BlastAlloy. BlastAlloy is strengthened with a fine dispersion ($\sim 0.1 \mu\text{m}$) of TiC and VC and contains between 2.5 and 6.5 wt.% Ni. The Ni is playing a dual role: (i) stabilizing a second phase austenitic iron and (ii) improving the interfacial adhesion between the carbide and the matrix. The resulting alloy is characterized by unusually high ductile fracture toughness and, as its name implies, is finding application in armored vehicles, ships, and airplanes, basically anywhere blast resistance is needed.

We gratefully acknowledge support of this work by ONR under Grant No. N00014-10-1-0838 and ARO under 421-20-18. We also thank Oleg Y. Kontsevoi and Arthur Freeman for supplying us with FLAPW charge densities and geometries for the interfaces.

*meberhar@mines.edu

- [1] R. F. W. Bader, *Atoms in Molecules. A Quantum Theory* (Clarendon, Oxford, 1990).
- [2] M. Eberhart, *Philos. Mag. B* **81**, 721 (2001).
- [3] T. Jones and M. Eberhart, *Int. J. Quantum Chem.* **110**, 1500 (2010).
- [4] T. E. Jones and M. E. Eberhart, *J. Chem. Phys.* **130**, 204108 (2009).
- [5] S. Dudy, J. Hartford, and B. I. Lundqvist, *Phys. Rev. Lett.* **85**, 1898 (2000).
- [6] R. Wu, A. Freeman, and G. Olson, *Science* **265**, 376 (1994).
- [7] R. Schweinfest, A. Paxton, and M. Finnis, *Nature (London)* **432**, 1008 (2004).
- [8] W. T. Geng, A. J. Freeman, and G. B. Olson, *Phys. Rev. B* **63**, 165415 (2001).
- [9] P. F. Zou and R. F. W. Bader, *Acta Crystallogr. Sect. A* **50**, 714 (1994).
- [10] D. Eberly, R. Gardner, B. Morse, S. Pizer, and C. Scharlach, *J. Math. Imaging Vis.* **4**, 353 (1994).
- [11] V. Tvergaard and J. W. Hutchinson, *Int. J. Solids Struct.* **39**, 3581 (2002).
- [12] J.-H. Lee, T. Shishidou, Y.-J. Zhao, A. J. Freeman, and G. B. Olson, *Philos. Mag. B* **85**, 3683 (2005).

- [13] T. Shishidou, J.-H. Lee, Y.-J. Zhao, A. J. Freeman, and G. B. Olson, *J. Appl. Phys.* **93**, 6876 (2003).
- [14] T. E. Jones, M. A. Sauer, and M. E. Eberhart, *Phys. Rev. B* **78**, 092104 (2008).
- [15] A. Hung, I. Yarovsky, J. Muscat, S. Russo, I. Snook, and R. O. Watts, *Surf. Sci.* **501**, 261 (2002).
- [16] G. Kresse and J. Furthmuller, *Comput. Mater. Sci.* **6**, 15 (1996).
- [17] J. P. Perdew, K. Burke, and M. Ernzerhof, *Phys. Rev. Lett.* **77**, 3865 (1996).
- [18] T. E. Jones, M. E. Eberhart, and D. P. Clougherty, *Phys. Rev. Lett.* **100**, 017208 (2008).
- [19] T. E. Jones and M. E. Eberhart, *Acta Crystallogr. Sect. A* **65**, 141 (2009).
- [20] M. Eberhart, *Acta Mater.* **44**, 2495 (1996).
- [21] See Supplemental Material at <http://link.aps.org/supplemental/10.1103/PhysRevLett.109.125506> for plots of the work of fracture versus the electron charge density at the second-neighbor Fe-Fe bond point and the Fe-C bond point in the Fe-carbide interfaces.
- [22] G. te Velde, F. Bickelhaupt, E. Baerends, C. F. Guerra, S. van Ginsbergen, J. Snijders, and T. Ziegler, *J. Comput. Chem.* **22**, 931 (2001).